JOURNAL OF ENERGY SYSTEMS

2023, 7(4)

2602-2052 DOI: 10.30521/jes.1316559 Research Article

Flow characteristics of two-dimensional impinging synthetic jets

Michiya Yasumiba *
Kogakuin University, Mechanical Engineering Department, Tokyo, Japan, am22068@ns.kogakuin.ac.jp
Koichi Nishibe
Tokyo City University, Mechanical Engineering Department, Tokyo, Japan, knishibe@tcu.ac.jp
Donghyuk Kang
Saitama University, Mechanical Engineering Department, Saitama, Japan, dhkang@mail.saitama-u.ac.jp
Kotaro Sato
Kogakuin University, Mechanical Engineering Department, Tokyo, Japan, at12164@ns.kogakuin.ac.jp

Submitted: 20.06.2023
Accepted: 20.10.2023
Published: 31.12.2023

* Corresponding Author

Abstract: We aimed to elucidate the behavior of impinging synthetic jets against the surface of a wall placed near the slot exit. Synthetic jets with various frequencies were used, and a rectangular body of finite length (target plate) was placed downstream of these jets. The flows were visualized by the smoke-wire method and numerical simulation, and the velocity distributions around the target plate were measured using a hot-wire anemometer. The flow fields of steady continuous jets and synthetic jets with unsteady characteristics were compared, and their flow characteristics were explored. We experimentally found that the flow field depends on the dimensionless target plate length and dimensionless frequency of the synthetic jet for a fixed distance from the slot to the target plate. Furthermore, at low frequencies, the behavior after impinging the target plate was similar to that observed for a continuous jet. Additionally, it has been confirmed that these results qualitatively agree with the numerical simulation results.

Keywords: *Flow visualization, Impinging jets, Numerical simulation, Synthetic jets, Velocity distribution*

Cite this paper as: Yasumiba, M., Nishibe, K., Kang, D., & Sato, K., Flow characteristics of two-dimensional impinging synthetic jets. *Journal of Energy Systems 2023; 7*(4): 327-338, DOI: 10.30521/jes.1097439

Nomenclature	
b_0	Slot width [m] (= 5.0 × 10⁻³ m)
$b_{1/2}$	Jet half-width [m] (distance from the *x* axis to the position indicating half of the maximum jet velocity)
x, y, z	Coordinate axes [m]
U_{s0}	Characteristic velocity in synthetic jets [m/s] ($= \frac{1}{T}\int_0^{\frac{T}{2}} u_0(t)dt$)
U_{c0}	Characteristic velocity in continuous jet [m/s]
u	Velocity along *x* axis [m/s]
u_0	Velocity along *x* axis at slot exit [m/s]
v	Velocity along *y* axis [m/s]
t	Time [s]
T	Period of velocity oscillation at slot exit [s]
v_m	Maximum value at distribution of velocity *v* along *y* axis [m/s]
x_{v_m}	*x*-axis position of jet center indicating v_m [m]
x_w	*x*-axis position of target plate [m]
X_w	Dimensionless *x*-axis position of target plate ($= x_w/b_0$)
s_w	Target plate length [m]
S_w	Dimensionless target plate length ($= s_w/b_0$)
f	Frequency [Hz]
f^*	Dimensionless frequency ($= fb_0/U_{s0} = 1/L_0$)
l_0	Stroke length [m] ($= U_{s0}/f$)
L_0	Dimensionless stroke length ($= U_{s0}/fb_0$)
c	Subscript denoting continuous jet
s	Subscript denoting synthetic jet

1. INTRODUCTION

Jet flows have been extensively studied for a long time [1–33]. For instance, steady continuous jets have been used to control flow. Recently, synthetic jets have been widely applied to flow control and to the driving source of small fluid machinery, replacing continuous jets to downsize and reduce the weight of equipment [4–23]. Regarding the fundamental behavior of synthetic jets, Nishibe et al. [8] compared synthetic and continuous jets, finding that the flow characteristics of two-dimensional synthetic jets under the free-jet condition in sufficient downstream are similar to those of continuous jets, including the unsteady characteristics. In addition, the jet formation position with a substantial flow rate depends on the dimensionless frequency.

A frequency exists for synthetic jets that are oscillatory flows, and it can determine the flow field in many cases. Recently, various methods to control the jet flow direction using frequency have been devised [12–17], highlighting the potential of synthetic jets to enable advanced flow control that cannot be realized using continuous jets. Impinging jets have a high heat transfer coefficient near the stagnation point when using a steady continuous jet. Therefore, they have been widely used for heating, cooling, drying, and removing dirt and moisture from the surface of various objects [24]. In recent years, synthetic and hybrid synthetic jets, which are suitable for miniaturization and weight reduction of devices, have been increasingly used as alternatives to continuous jets for cooling heating devices such as computer processors [25–31]. Malingham and Glezer [25] and Pavlova and Amitay [26] experimentally demonstrated that for a fixed Reynolds number, the heat transfer coefficient and cooling effect are higher for collisional synthetic jets than for conventional collisional stationary jets. Pavlova and Amity [26] also reported that the heat transfer performance is higher for high-frequency synthetic jets when the orifice-to-wall distance is small and for low-frequency synthetic jets when the orifice-to-wall distance is large. Chaudhari et al. [27] and Wang et al. [28] discussed the influence of the orifice geometry to generate impinging synthetic jets and the distance from the slot exit to a target on the cooling performance. Furthermore, Xu et al. [29] investigated the combined effects of the distance from the orifice to target wall for synthetic jets and the wall surface temperature of the heating element by visualization experiments using particle image velocimetry. When the orifice-to-wall distance is relatively large, the intensity of the vortex ring generated downstream of the orifice decreases before impinging the target plate, completely losing coherence and consequently reducing the cooling performance. All the above-mentioned studies considered fixed target plate sizes, and scarce research is available on geometric parameters that may be important for cooling applications. Hence, the influence of the relative length (relative size) of the target plate and dimensionless frequency on the flow characteristics should be unveiled to improve the applicability of synthetic jets.

We aim to elucidate the behavior of synthetic jets when the target plate is placed near the slot. Plane synthetic jets are generated at a fixed distance from the slot to the target plate, and the influence of both the target plate length and frequency on the time-averaged flow field are experimentally investigated. The relation between jet behavior (e.g., flow direction, vortex formation) and dimensionless frequency for various relative target plate lengths is analyzed. The flow characteristics of impinging synthetic/continuous jets are evaluated according to their similarities and differences. Simple numerical calculations assuming two-dimensional flow are performed to confirm the generality of the experimental results, and the experimental and numerical results are compared qualitatively.

2. EXPERIMENTAL AND METHOD

Fig. 1 shows schematic diagrams of the experimental setup from the front and side views. The working fluid was air, and the pressure in the plenum tank at the center of the apparatus show in Fig. 1(b) was

unsteady because of the oscillating speaker. As a result, the pressure in the cavity located near the center in Fig. 1(a) was also unsteady, which could create an oscillatory flow in the slot. The flow measurement area was sandwiched between two acrylic plates on the top and bottom, and the aspect ratio of the slot exit cross-section was 20. The flow field test area was $80b_0$ along the *x* axis and $200b_0$ along the *y* axis. A sine wave was generated by the Audacity software to generate a signal that was amplified and then input to a loudspeaker. A blower and inverter were used to generate the continuous jet.

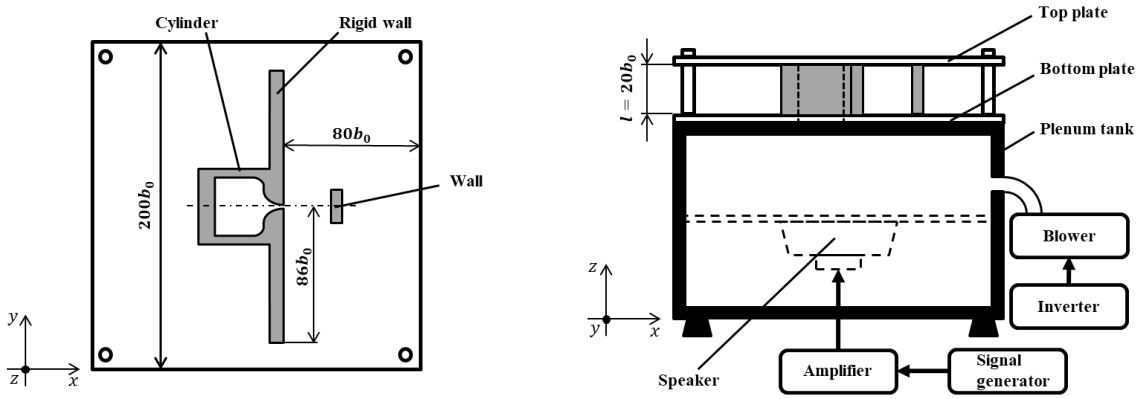

(a) *(b)*

Figure 1. Schematic of experimental equipment: (a)Front view, (b) side view.

Fig. 2 shows a magnified view of the geometry of the slot exit and coordinate system. The origin was defined as the center of the slot exit on the central section along the *z* axis, and velocity measurements were taken on the central section along the same axis. The slot exit velocity, U_{s0}, of the synthetic jet was calculated as follows [5]:

$$U_{s0} = \frac{1}{T}\int_0^{\frac{T}{2}} u_0(t)dt \qquad (1)$$

Hence, velocity U_{s0} was calculated by periodic averaging of only the velocity at the origin during the jet process because the momentum does not produce flow field during suction [5]. For a continuous jet, the time-averaged velocity at the origin was defined as the slot exit velocity, U_{c0}.

We obtained the results at $U_{s0} = U_{c0} = 4.5$ m/s. The smoke-wire method was applied to visualize the flow field, and the jet behavior was captured by a digital camera (Sony Vlog Camera ZV-1) using a halogen light source at 480 fps. A hot-wire anemometer (Kanomax Model 7250) was used to measure the velocity. In this experiment, the distribution of velocity v along the y axis was measured at intervals of 2 mm for $2 \leq x \leq 200$ mm at $y = 50$ and 100 mm. The x-axis position at which time-averaged velocity v showed the maximum value, v_m, at $y = 50$ mm was denoted as x_{v_m}. From the digital camera photographs of flow, the flow field was obtained as a time-averaged pattern by making a frame chart and superimposing the frames for 1 s for the continuous jet and 10 cycles for the synthetic jet.

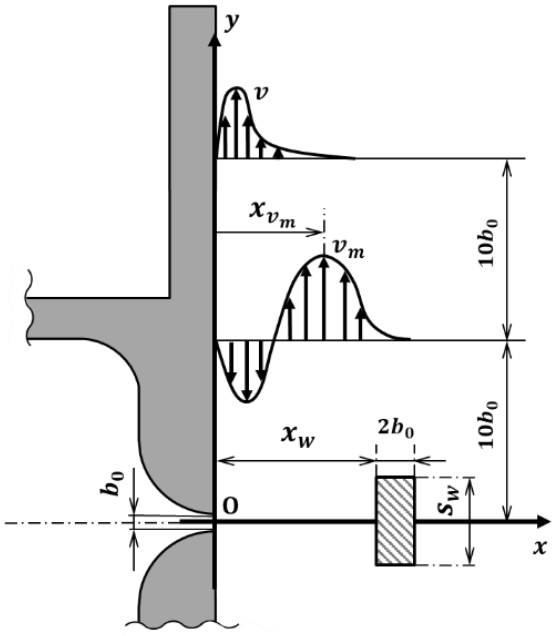

Figure 2. Diagram of slot exit.

This experiment was performed under constant conditions with a relative distance $X_w(= x_w/b_0) = 10$ from the slot to the target plate.

3. NUMERICAL SIMULATIONS

Fig. 3 shows an enlarged view of the mesh near the region and slot for numerical simulations. Numerical calculations were performed using Ansys Fluent (version 2021 R1), a general-purpose thermo-fluid analysis software with a fluid unstructured grid. The figure shows an example with a dimensionless target plate length S_w $(= s_w/b_0) = 2$. The boundary conditions included the flow velocity at the slot inlet, total pressure at the upper and lower boundaries, static pressure at the outlet of the computational domain, non-slip conditions at the sides of the slot, and rigid wall and wall surface.

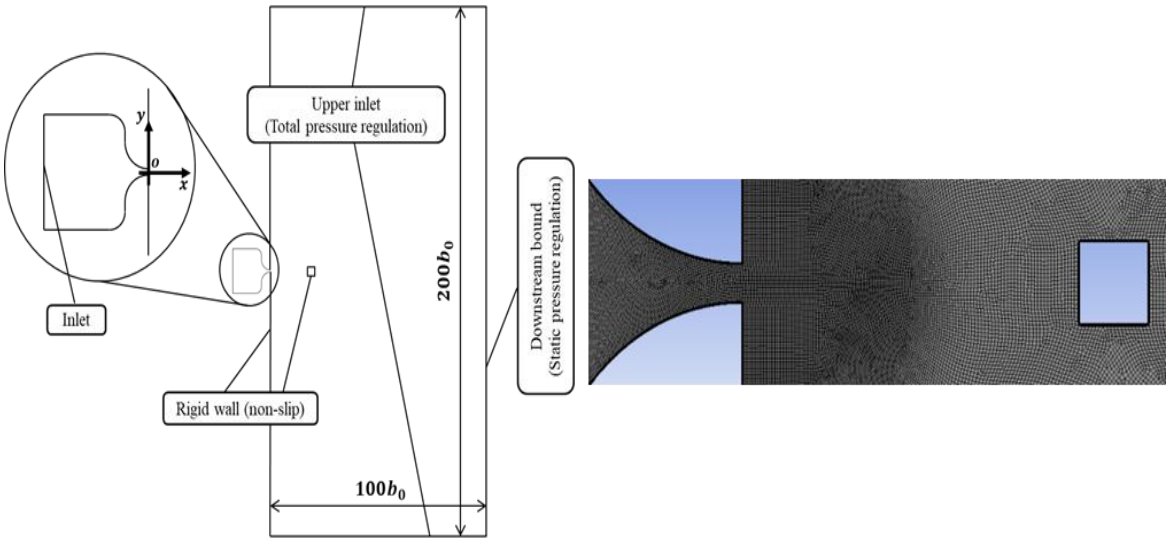

Figure 3. Domain and boundary conditions in numerical analysis with typical mesh near slot for $S_w = 2$.

Pablo et al. [32] examined the shear stress produced by steady continuous jet impingement, performing both experiments and numerical simulations. They validated the local mesh density and assessed the computational model with five different turbulence modeling techniques to determine the most accurate predictor of this effect. Hui et al. [33] discussed turbulence models suitable for representing the motion of synthetic jets. Given that the purpose of this study is to illustrate the approximate behavior of synthetic jets in the presence of a target plate length, we assumed a two-dimensional flow in our simulations and limited our comparative discussion between the experimental and numerical results to qualitative aspects. Considering the insights from prior research, preliminary calculations, computational costs, and a comprehensive evaluation, we selected the k-ε turbulence model for this study. Additionally, regarding mesh dependency, we determined that approximately 300,000 mesh elements were sufficient based on preliminary calculations conducted with various numbers of meshes, referencing prior research [32]. For time-averaging in computational fluid dynamics, the time-averaged value was obtained over 1 s for the continuous jet and over 10 cycles for the synthetic jet.

3. RESULTS AND DISCUSSIONS

Figs. 4,5,6 show typical time-averaged flow patterns for the target plate placed at $X_w = 10$ and dimensionless target plate lengths $S_w = 13, 5$, and 2, respectively. In these figures, panels (a) show flow visualization using the smoke-wire method, while panels (b) show the distribution of absolute values of dimensionless y-axis velocity $|v|/U_{i0}$ (i = c or s) measured experimentally at $y/b_0 = 10$ and 20. In addition, panels (c) show the dimensionless velocity contour plot calculated numerically, and panels (d) show the dimensionless velocity distribution along the y axis calculated numerically at $y/b_0 = 10$ and 20. The results are shown for continuous jets in (i) and for synthetic jets in (ii) for $f^* = 1.11 \times 10^{-2}$ ($f = 10$ Hz, $L_0 = 90$), (iii) for $f^* = 3.33 \times 10^{-2}$ ($f = 30$ Hz, $L_0 = 30$), and (iv) for $f^* = 6.67 \times 10^{-2}$ ($f = 60$ Hz, $L_0 = 15$), where f^* ($= fb_0/U_{s0}$) is the dimensionless frequency and L_0 ($= U_{s0}/fb_0 = 1/f^*$) is the dimensionless stroke length. Counterclockwise vortices are defined as positive and clockwise vortices as negative, and the direction of rotation of the vortices confirmed by video observation is depicted in panels (a) of Figs. 4–6.

Consider Fig. 4(a) with photographs for target plate length $S_w = 13$. Two recirculation zones are formed between the slot sidewall and target plate for the (i) continuous jet and synthetic jets with (ii) $f^* = 1.11 \times 10^{-2}$, (iii) $f^* = 3.33 \times 10^{-2}$, and (iv) $f^* = 6.67 \times 10^{-2}$. In Fig. 4(c), the numerical and experimental results agree qualitatively. For $S_w = 13$, the target plate is relatively long, and both the continuous and synthetic jets (for various frequencies) form recirculation zones. Then, wall jet formation is observed on the surface of the slot side. Comparing the experimental and numerical calculation results for the velocity distributions in Figs. 4(b, d), a qualitative difference occurs for $y/b_0 = 10$. This is because the experimental data are obtained from a hot-wire anemometer and expressed as absolute values. Therefore, both results are in good agreement qualitatively. From the time-averaged velocity distribution in Fig. 4, the formation of an attached wall jet on the slot side wall can be confirmed under all conditions for $y/b_0 = 20$.

All the results in Figs. 4,5,6 show that condition (iv) $f^* = 6.67 \times 10^{-2}$ has twice the frequency of condition (iii) $f^* = 3.33 \times 10^{-2}$, while no significant difference is observed between conditions (iii) and (iv). Under constant X_w, the flow pattern may become independent of the dimensionless frequency once a certain value is exceeded, but this finding remains to be verified over a wide range of conditions in future work.

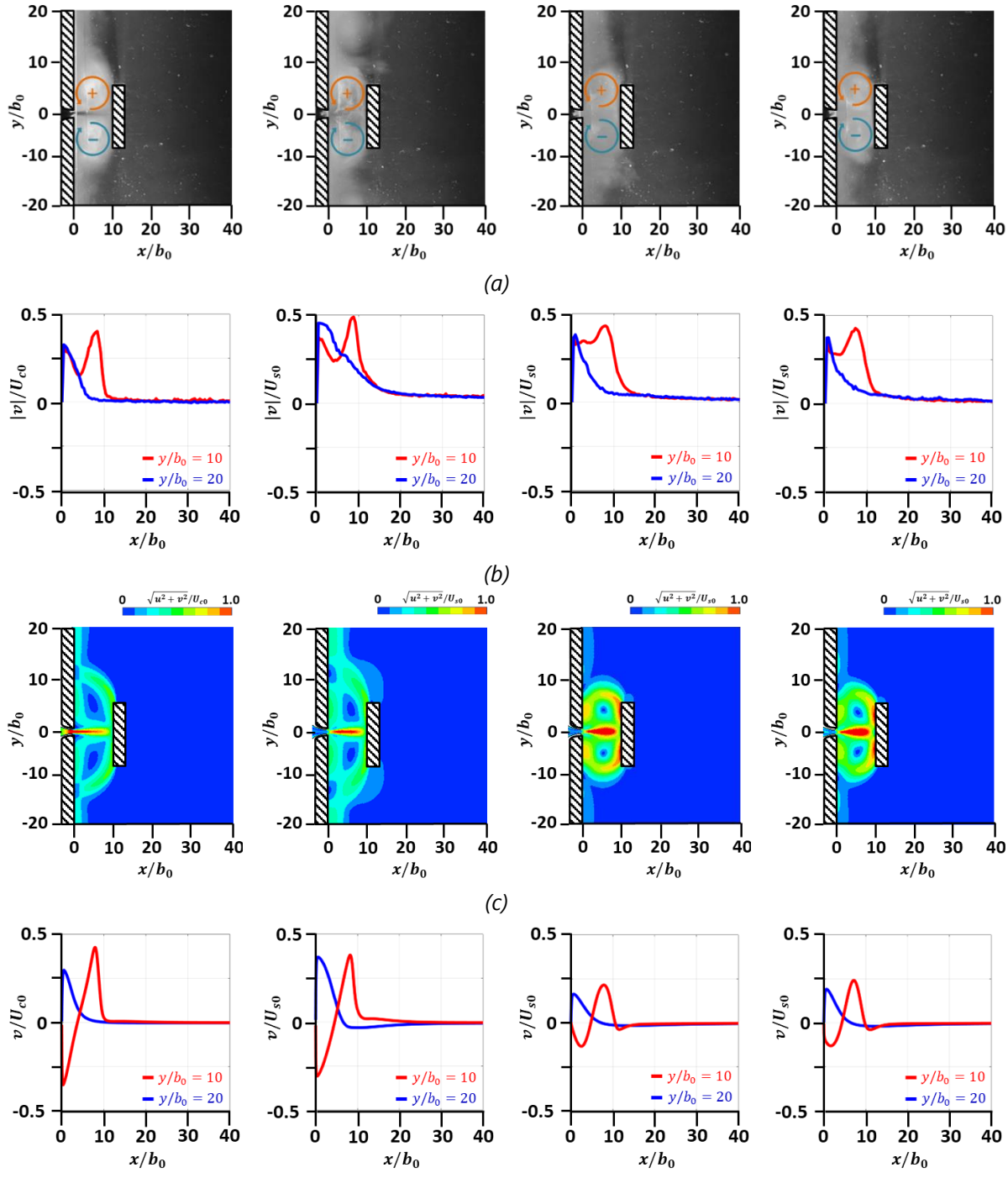

(i) Continuous jet *(ii)* $f^* = 1.11 \times 10^{-2}$ $(f = 10\ Hz, L_0 = 90)$ *(iii)* $f^* = 3.33 \times 10^{-2}$ $(f = 30\ Hz, L_0 = 30)$ *(iv)* $f^* = 6.67 \times 10^{-2}$ $(f = 60\ Hz, L_0 = 15)$

Figure 4. Visualization of synthetic and continuous jets by smoke-wire method and numerical analysis and velocity distribution measured at $y/b_0 = 10$ *and* $20.\left[U_{s0} = U_{c0} = 4.5\frac{m}{s}, b_0 = 5.0 \times 10^{-3}\ m, X_w = 10, S_w = 13\right]$*: (a) Flow visualization by smoke-wire method, (b) dimensionless velocity along y axis at* $y/b_0 = 10$ *and* 20 *from experiment, (c) dimensionless velocity along y axis at* $y/b_0 = 10$ *and* 20 *from computational fluid dynamics, (d) dimensionless velocity contour from computational fluid dynamics.*

Fig. 5 shows the results for $S_w = 5$, which are in approximate agreement with those for $S_w = 13$ shown in Fig. 4.

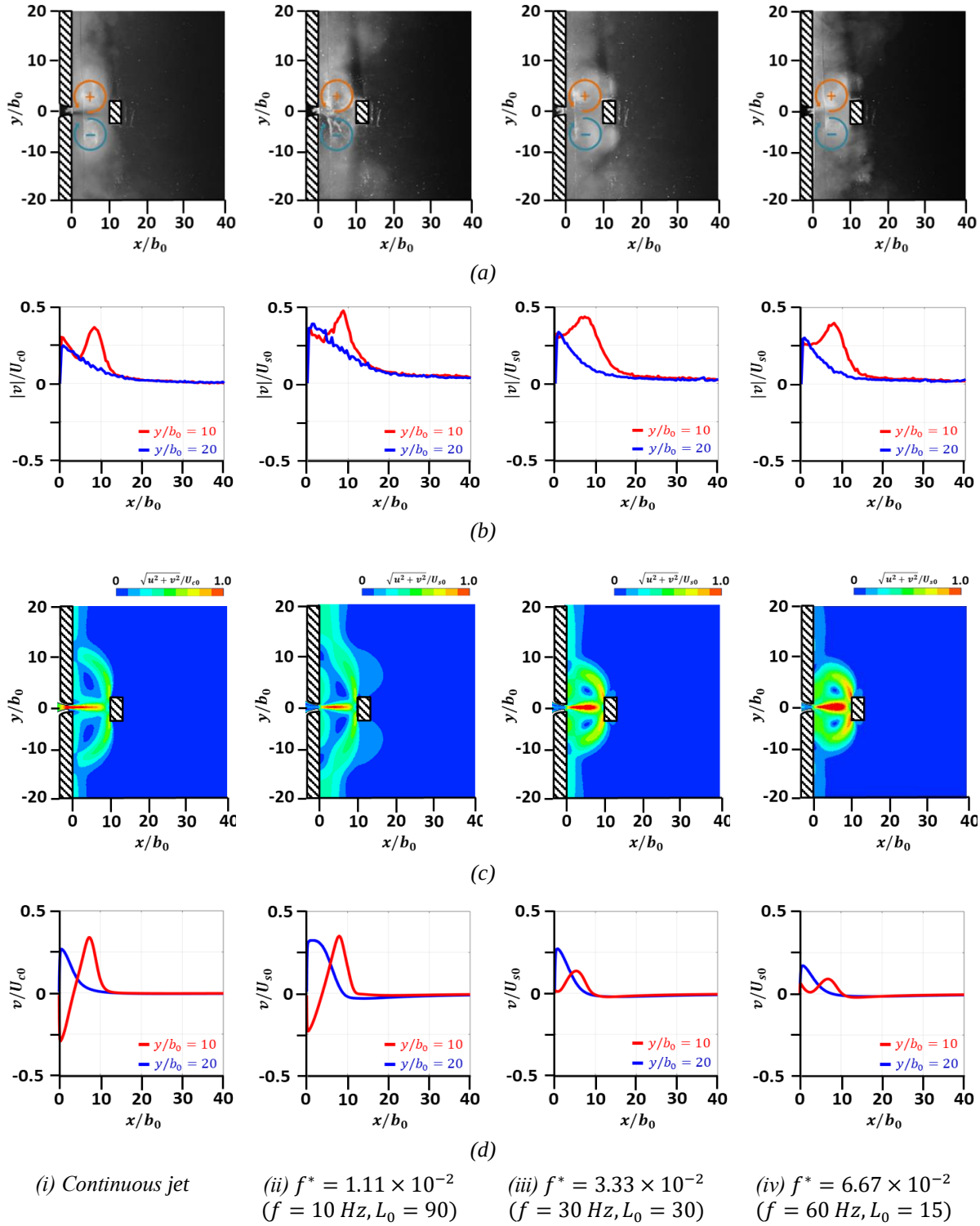

(i) Continuous jet | *(ii)* $f^* = 1.11 \times 10^{-2}$ $(f = 10\ Hz, L_0 = 90)$ | *(iii)* $f^* = 3.33 \times 10^{-2}$ $(f = 30\ Hz, L_0 = 30)$ | *(iv)* $f^* = 6.67 \times 10^{-2}$ $(f = 60\ Hz, L_0 = 15)$

Figure 5. Visualization of synthetic and continuous jets by smoke-wire method and numerical analysis and velocity distribution measured at $y/b_0 = 10$ *and* $20.[U_{s0} = U_{c0} = 4.5\ m/s, b_0 = 5.0 \times 10^{-3}\ m, X_w = 10, S_w = 5]$*: (a) Flow visualization by smoke-wire method, (b) Dimensionless velocity along y axis at* $y/b_0 = 10$ *and* 20 *from experiment, (c) Dimensionless velocity along y axis at* $y/b_0 = 10$ *and* 20 *from computational fluid dynamics, (d) Dimensionless velocity contour from computational fluid dynamics.*

Although S_w in Fig. 5 is less than half of that in Fig. 4, the recirculation zone size and approximate shape of the time-averaged velocity distribution have negligible differences. Previous studies [1,8] and preliminary experiments have shown that the dimensionless half-width of the jet at $x/b_0 = 10$ in a free

jet is approximately $b_{1/2}/b_0 = 1.5$. $S_w = 5$ (i.e., dimensionless distance from *x* axis to target plate edge of 2.5) is considered large compared with the jet half-width at $x/b_0 = 10$. Although the difference between the half-width and jet width should be noted, the momentum of the jet within the half-width accounts for about 85% of the total momentum of the jet. Hence, considering the jet half-width as the actual jet width is convenient. Under this condition, when the target plate length, S_w, is larger than the jet half-width, $b_{1/2}/b_0$, the flow field does not sensitively depend on S_w.

Fig. 6 shows the results for $S_w = 2$, which indicates a very short target plate. For the (i) continuous jet in Figs. 6(a,c), the flow pattern is different from the results shown in Figs. 4 and 5. The jet separates into two after impinging the target plate and flows with a velocity distribution in the oblique direction. The formation of a recirculation zone in the test section is not observed for the continuous jet under this condition, in which target plate length S_w is small compared with the jet half-width. The time-averaged flow for the synthetic jet with (ii) $f^* = 1.11 \times 10^{-2}$, where the dimensionless stroke in the synthetic jet is large, is similar to that for the continuous jet, with an apparent separation into two jets. Under this condition, in which the dimensionless stroke is relatively large for the distance from the slot to the target plate (i.e., relatively small dimensionless frequency), the vortex pairs generated near the slot during ejection pass through the target plate owing to mutual translational motion. On the other hand, during suction, the flow is drawn from the entire flow field. Hence, two separate jet-like velocity components remain when averaging over time. For the synthetic jet with (iii) $f^* = 3.33 \times 10^{-2}$ and (iv) $f^* = 6.67 \times 10^{-2}$, as the dimensionless stroke is relatively short (i.e., relatively large dimensionless frequency), the vortex pairs of the next period are generated before they pass the target and gradually catch up with each other and merge with the same rotational direction. Gradually, the vortex pairs in the same rotational direction merge (roll up). This process is repeated to create vortex clusters symmetrically along the *x* axis, forming a recirculation zone with different orientations at the top and bottom. The behavior for cases (iii) and (iv) can be understood as that characterizing synthetic jets that emit vortices discretely. The recirculation zone sizes observed for cases (iii) and (iv) with $S_w = 2$ in Fig. 6 are larger than those with $S_w = 13$ in Fig. 4 and $S_w = 5$ in Fig. 5. However, the recirculation zone size differs for the experiment and computational fluid dynamics. The quantitative difference between the two analyses is most likely due to the numerical simulation assuming a two-dimensional flow, while the experimental simulation assumes a strictly three-dimensional flow with the test section sandwiched between two plates. However, because the establishment of a simulation code and numerical prediction were not the main objectives of this study and given the high computational cost, numerical calculations were used only to verify the phenomena observed in the experiments. Nevertheless, the differences in target plate lengths are relatively small, suggesting that the recirculation zone size does not notably depend on S_w under the considered conditions.

Comparing the time-averaged velocity distributions in Figs. 6(b,d), for the (i) continuous jet and synthetic jet with (ii) $f^* = 1.11 \times 10^{-2}$, the curve profiles are considerably different between the experimental and numerical results. This is due to the difference in the heading angle of the jet motion after it splits into two between the experiment and calculation. We confirm that the results are in qualitative agreement, but the center position of *y*-axis velocity v of the jet in the experiment is downshifted compared with the calculated value. For conditions (i) and (ii), the maximum value of velocity $|v|/U_{i0}$ is located well behind the target plate location, $x/b_0 = 10$, which is clearly different from the results obtained for conditions (iii) and (iv). Comparing the experimental results in Fig. 6(a) and numerical results in Fig. 6(c) for (iii) $f^* = 3.33 \times 10^{-2}$ and (iv) $f^* = 6.67 \times 10^{-2}$, the experimental and numerical results are in qualitative agreement, although the recirculation zone appears larger in the experiment than in the calculation.

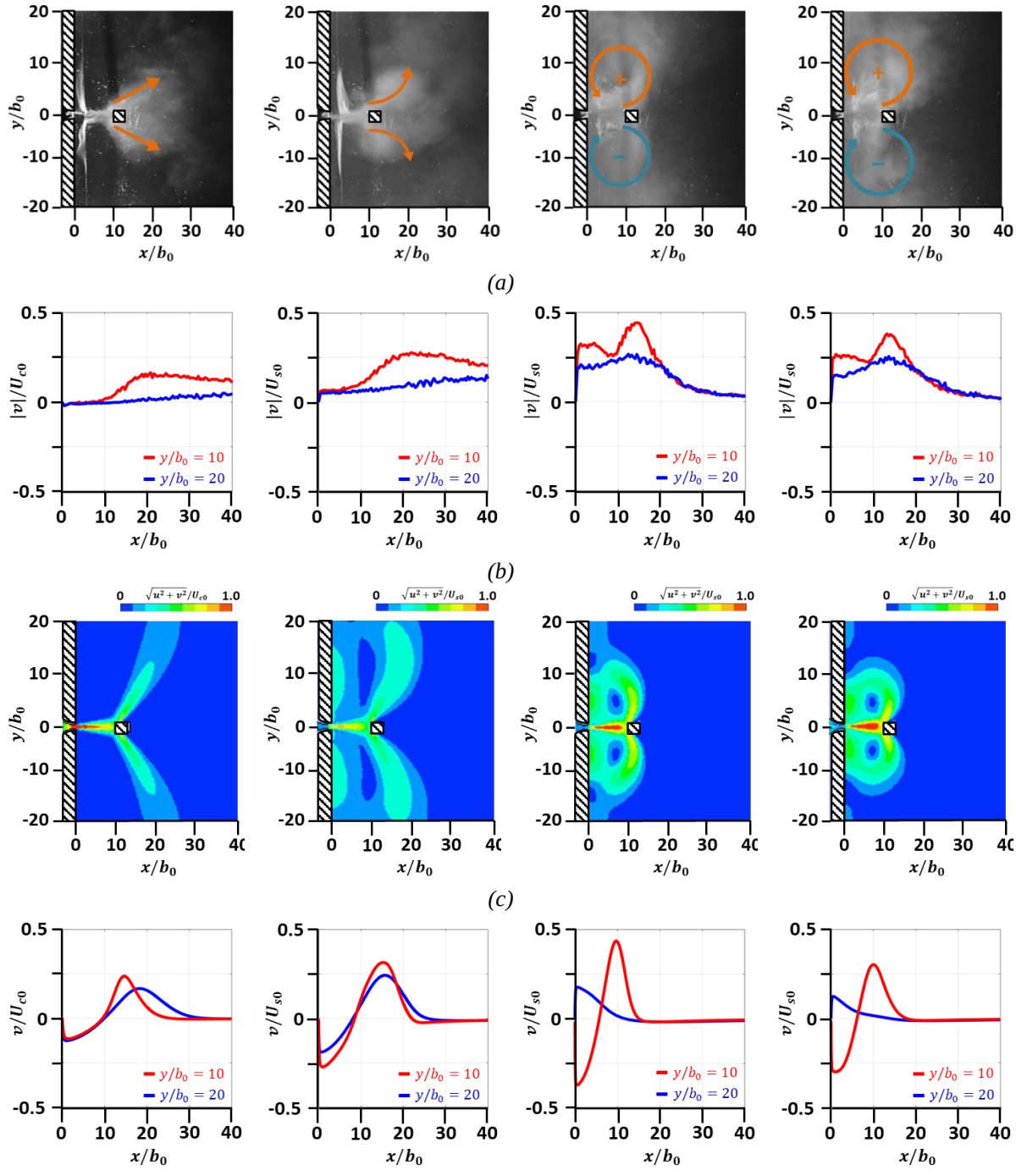

(i) Continuous jet *(ii)* $f^* = 1.11 \times 10^{-2}$ $(f = 10\ Hz, L_0 = 90)$ *(iii)* $f^* = 3.33 \times 10^{-2}$ $(f = 30\ Hz, L_0 = 30)$ *(iv)* $f^* = 6.67 \times 10^{-2}$ $(f = 60\ Hz, L_0 = 15)$

Figure 6. Visualization of synthetic and continuous jets by smoke-wire method and numerical analysis and velocity distribution measured at $y/b_0 = 10$ *and* $20.[U_{s0} = U_{c0} = 4.5\ m/s, b_0 = 5.0 \times 10^{-3}\ m, X_w = 10, S_w = 2]$*: (a) Flow visualization by smoke-wire method, (b) dimensionless velocity along y axis at* $y/b_0 = 10$ *and* 20 *from experiment, (c) dimensionless velocity along y axis at* $y/b_0 = 10$ *and* 20 *from computational fluid dynamics, (d) dimensionless velocity contour from computational fluid dynamics.*

Fig. 7 shows the relation between the target plate length and *x*-axis position of the jet center. The horizontal axis indicates the nondimensional length of the target plate, S_w, and the vertical axis indicates the *x*-axis coordinate, x_{v_m}, at which the time-averaged velocity distribution along the *y* axis measured at $y/b_0 = 10$ reaches its maximum v_m. Fig. 7(a, b) show the experimental and numerical results, respectively. The results for $X_w = 10$, which corresponds to the location of the target plate, are indicated

by dashed lines in the graphs. There are quantitative differences caused by the heading angle of jets between the experimental and numerical results, but a qualitative agreement is observed. In Fig. 7(a) showing the experimental results, the *x*-axis position of the jet center lies between the slot and target plate in the four conditions for $S_w \geq 4$. On the other hand, for $S_w = 2$, the jet center lies behind the target plate. Moreover, x_{v_m} for $f^* = 1.11 \times 10^{-2}$ is approximately 1.7 times larger than that for $f^* = 6.67 \times 10^{-2}$, indicating that the flow direction changes substantially with frequency. In addition, $S_w = 2$, there is a large difference in the case of continuous jet and $f^* = 1.11 \times 10^{-2}$ and in the case of $f^* = 3.33 \times 10^{-2}$ and $f^* = 6.67 \times 10^{-2}$. However, the difference becomes smaller when $S_w = 3$ and negligible when $S_w = 4$. In other words, when an object with a relatively small target length S_w is placed downstream of a low-frequency synthetic jet, the jet splits into two and travels at an angle, as shown in Figs. 6(a, c). This is confirmed by velocity measurements.

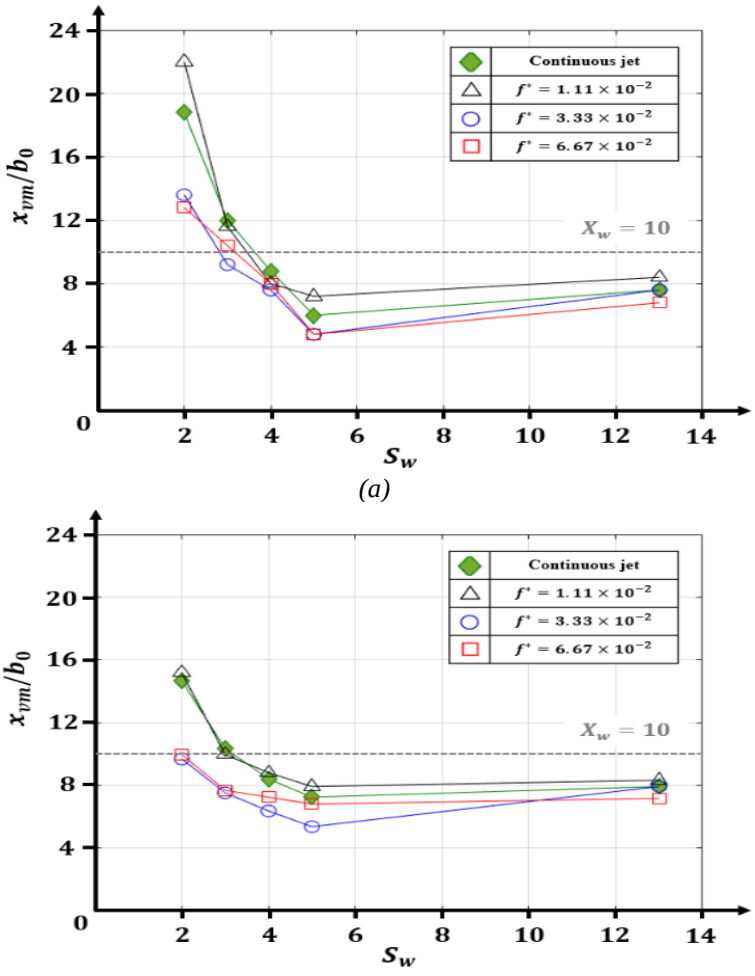

Figure 7. Relation between target length and x-axis position of jet center for y-axis velocity. $[U_{s0} = U_{c0} = 4.5\ m/s, b_0 = 5.0 \times 10^{-3}\ m, X_w = 10, y/b_0 = 10]$*: (a) Experiment, (b) computational fluid dynamics.*

4. CONCLUSION

We aimed to elucidate the behavior of a synthetic jet considering a target plate of finite length placed near the slot. The effects of target plate length and frequency on the time-averaged flow field were investigated under constant dimensionless distance $X_w = 10$ from the slot to the target plate. We can draw the following main conclusions considering the conditions in this study:

1) For a relatively long target plate (i.e., $S_w \geq 5$), both continuous and synthetic jets produce a recirculation zone between the slot side wall and target plate, and y-axis wall jets are formed on the surface of the slot side wall.
2) When the dimensionless frequency of the synthetic jet is $f^* \geq 3.33 \times 10^{-2}$ for any target plate length and considered experimental conditions, a recirculation zone is formed between the slot side wall and target plate. In addition, the zone size does not considerably depend on the target plate length or dimensionless frequency.
3) For a short target plate (i.e., $S_w = 2$), the continuous and synthetic jets with $f^* = 1.11 \times 10^{-2}$ separate into two jets after the jets collide the target plate and then travel in an oblique direction.
4) In qualitative terms, the experimental results are in good agreement with the numerical calculations obtained from a simple model.

Acknowledgement

We are grateful to Takumi Ito (Kogakuin University) for the assistance in conducting this study. This work was supported by JSPS KAKENHI under Grant number 21K03862. We would like to thank Editage (www.editage.com) for English language editing.

REFERENCES

[1] Forthman, E. Turbulent jet expansion. *Ingenieur-Archiv* 1934; *V*: 1-19.
[2] Rajaratnam, N. Turbulent Jets. Amsterdam, THE NETHERLANDS: Elsevier Scientific Publishing Company, 1976.
[3] Shakouchi, T. Jet Flow Engineering. Tokyo, JAPAN: Morikita Publishing, 2004.
[4] Glezer, A., Amitay, M. Synthetic jets. *Annual Review of Fluid Mechanics* 2002; *34*(1): 503-529. DOI: 10.1146/annurev.fluid.34.090501.094913.
[5] Holman, R, Utturkar, Y, Mittal, R, Smith, BL, Cattafesta, L. Formation criterion for synthetic jets. *AIAA Journal* 2005; *43*(10): 2110-2116. DOI: 10.2514/1.12033.
[6] Smith, BL, Swift, GW. A comparison between synthetic jets and continuous jets. *Experiments in Fluids* 2003; *34*(4): 467-472. DOI: 10.1007/s00348-002-0577-6.
[7] Tang, H, Zhong, S. 2D numerical study of circular synthetic jets in quiescent flows. *Aeronautical Journal* 2005; *109*(1092): 89-97. DOI: 10.1017/S0001924000000592.
[8] Nishibe, K, Fujita, Y, Sato, K, Yokota, K, Koso, T. Experimental and numerical study on the flow characteristics of synthetic jets. *Journal of Fluid Science and Technology* 2011; *6*(4): 425-436. DOI: 10.1299/jfst.6.425.
[9] Koso, T, Morita, M. Effects of stroke and Reynolds number on characteristics of circular synthetic jets. *Journal of Fluid Science and Technology* 2014; *9*(2): JFST0021. DOI: 10.1299/jfst.2014jfst0021.
[10] Koso, T, Matsuda, S, Masuda, H, Akahoshi, T. Effect of stroke on structure of vortex ring array in circular synthetic jets. *Journal of Fluid Science and Technology* 2014; *9*(3): JFST0034. DOI: 10.1299/jfst.2014jfst0034.
[11] Nishibe, K, Fujiwara, T, Ohue, H, Takezawa, H, Sato, K, Yokota, K. Synthetic jet actuator using bubbles produced by electric discharge. *Journal of Fluid Science and Technology* 2014; *9*(3): JFST0033. DOI: 10.1299/jfst.2014jfst0033.
[12] Smith, BL, Glezer, A. Jet vectoring using synthetic jets. *Journal of Fluid Mechanics* 2002; *458*: 1-34. DOI: 10.1017/S0022112001007406.
[13] Watabe, Y, Sato, K, Nishibe, K, Yokota, K. The influence of an asymmetric slot on the flow characteristics of synthetic jets. In: Proceedings of the 5th International Conference on Jets, Wakes and Separated Flows (ICJWSF2015); 2016: Springer International Publishing, pp. 101-107.
[14] Kobayashi, R, Nishibe, K, Watabe, Y, Sato, K, Yokota, K. Vector control of synthetic jets using an asymmetric slot. *Journal of Fluids Engineering* 2018; *140*(5): 051102. DOI: 10.1115/1.4038660.
[15] Kobayashi, R, Terakado, H, Sato, K, Taniguchi, J, Nishibe, K, Yokota, K. Behavior of plane synthetic jets generated by an asymmetric stepped slot. *International Journal of Fluid Machinery and Systems* 2020; *13*(1): 253-265. DOI: 10.5293/IJFMS.2020.13.1.253.

[16]Kobayashi, R, Watabe, Y, Tamanoi, Y, Nishibe, K, Kang, D, Sato, K. Jet vectoring using secondary Coanda synthetic jets. *Mechanical Engineering Journal* 2020; *7*(5): 20-00215. DOI: 10.1299/mej.20-00215.
[17]Zhang, Q, Tamanoi, Y, Kang, D, Nishibe, K, Yokota, K, Sato, K. Influence of amplitude of excited secondary flow on the direction of jets. *Transactions of the Japan Society for Aeronautical and Space Sciences* 2023; *66*(2): 37-45. DOI: 10.2322/tjsass.66.37.
[18]Amitay, M, Smith, DR, Kibens, V, Parekh, DE, Glezer, A. Aerodynamic flow control over an unconventional airfoil using synthetic jet actuators. *AIAA Journal* 2001; *39*(3): 361-370. DOI: 10.2514/2.1323.
[19]Haider, BA, Durrani, N, Aizud, N, Zahir, S. Aerodynamic stall control of a generic airfoil using synthetic jet actuator. *International Journal of Aerospace and Mechanical Engineering* 2010; *4*(9): 788-793. DOI: 10.5281/zenodo.1083649.
[20]Yen, J, Ahmed, NA. Parametric study of dynamic stall flow field with synthetic jet actuation. *Journal of Fluids Engineeering* 2012; *134*(7): 071106. DOI: 10.1115/1.4006957.
[21]Duvigneau, R, Hay, A, Visonneau, M. Optimal location of a synthetic jet on an airfoil for stall control. *Journal of Fluids Engineering* 2007; *129*(7): 825-833. DOI: 10.1115/1.2742729.
[22]Ishizawa, T, Sato, K, Nishibe, K, Yokota, K. Performance characteristics of a fan using synthetic jets. In: Proceedings of the 5th International Conference on Jets, Wakes and Separated Flows (ICJWSF2015); 2016: Springer International Publishing, pp. 109-115.
[23]Nishibe, K, Nomura, Y, Noda, K, Ohue, H, Sato, K. Influence of stroke on performance characteristics of synthetic jet fan. *Journal of Applied Fluid Mechanics* 2018; *11*(4): 945-956. DOI: 10.29252/jafm.11.04.28493.
[24]Kanamori, A, Hiwada, M, Senaha, I, Oyakawa, K. Effect of orifice configuration on flow behavior and impingement heat transfer. *The Japan Society of Mechanical Engineers Essay Collection (Part B)* 2011; *77*(775): 456-464 (in Japanese). DOI: 10.1299/kikaib.77.456.
[25]Malingham, R, Glezer, A. Design and thermal characteristics of a synthetic jet ejector heat sink. *Journal of Electronic Packaging* 2005; *127*: 172-177. DOI: 10.1115/1.1869509.
[26]Pavlova, A, Amitay, M. Electronic cooling with synthetic jet impingement. *ASME Journal of Heat and Mass Transfer* 2006; *128*(9): 897-907. DOI: 10.1115/1.2241889.
[27]Chaudhari, M, Puranik, B, Agrawal, A. Effect of orifice shape in synthetic jet-based impingement cooling. *Experimental Thermal and Fluid Science* 2010; *34*(2): 246-256. DOI: 10.1016/j.expthermflusci.2009.11.001.
[28]Wang, L, Feng, LH, Xu, Y, Xu, Y, Wang, JJ. Experimental investigation on flow characteristics and unsteady heat transfer of noncircular impinging synthetic jets. *International Journal of Heat and Mass Transfer*, 2022; *190*: 122760. DOI: 10.1016/j.ijheatmasstransfer.2022.122760.
[29]Xu, Y, Moon, C, Wang, JJ, Penyazkov, OG, Kim, KC. An experimental study on the flow and heat transfer of an impinging synthetic jet. *International Journal of Heat and Mass Transfer* 2019; *144*: 118626. DOI: 10.1016/j.ijheatmasstransfer.2019.118626.
[30]Silva-Llanca, L, Ortega, A, Rose, I. Experimental convective heat transfer in a geometrically large two-dimensional impinging synthetic jet. *International Journal of Thermal Sciences* 2015; *90*: 339-350. DOI: 10.1016/j.ijthermalsci.2014.11.011.
[31]Trávníček, Z, Vít, T. Impingement heat/mass transfer to hybrid synthetic jets and other reversible pulsating jets. *International Journal of Heat and Mass Transfer* 2015; *85*: 473-487. DOI: 10.1016/j.ijheatmasstransfer.2015.01.125.
[32]Pablo, M, F, Koldo, P, P, Unai, F, G, Ekaitz, Z, Josu, S. Experimental and numerical modeling of an air jet impingement system. *European Journal of Mechanics / B Fluids* 2022; *94*: 228-245. DOI: 10.1016/j.euromechflu.2022.03.005.
[33]Hui, T, Shan, Z. 2D numerical study of circular synthetic jets in quiescent flows. *The Aeronautical Journal* 2005; *2938*: 89-97. DOI: 10.1017/S0001924000000592.